Hindawi
Geofluids
Volume 2022, Article ID 1968938, 15 pages
https://doi.org/10.1155/2022/1968938

Research Article

Study on the Effect of Rock Strength on the Macro-Meso Shear Behaviors of Artificial Rock Joints

Yujing Jiang,[1,2] Sunhao Zhang,[1,2] Hengjie Luan,[1,2] Qinglin Shan,[1,2] Baocheng Li,[1,2] Dong Wang,[1,2] and Chuanyang Jia[3]

[1]*State Key Laboratory of Mining Disaster Prevention and Control Co-founded by Shandong Province and the Ministry of Science and Technology, Shandong University of Science and Technology, Qingdao 266590, China*
[2]*College of Energy and Mining Engineering, Shandong University of Science and Technology, Qingdao 266590, China*
[3]*School of Civil Engineering and Architecture, Linyi University, Linyi 276000, China*

Correspondence should be addressed to Qinglin Shan; skd995946@sdust.edu.cn

Received 23 July 2021; Accepted 11 October 2021; Published 16 March 2022

Academic Editor: Bailu Teng

Understanding the shear properties of joints of rock masses is of great importance for engineering disaster prevention and control. In this paper, a systematic study of the macroscopic shear properties of joints of rock masses with different strengths is carried out using a combination of indoor tests and PFC^{2D} numerical simulations. The results show that (i) the shear stress curve of low-strength rock joints is strain-softening type, while high-strength rock joints are strain-hardening type, and high-strength rock joints are more sensitive to the change of roughness. (ii) With the increase of JRC, the damage mode of different strength rock joints gradually changes from "abrasion" to "abrasion + gnawing," and the damage characteristics of the surface of high-strength rock joints are more significant. (iii) The contact force between particles is mainly concentrated on the joints. At the beginning of shear, the contact force is mainly distributed on the second-order roughness and gradually concentrated on the first-order roughness as the shear progresses. Compared with the low-strength rock joints, the contact force on the high-strength rock joints is larger and more widely distributed. (iv) Due to the change of contact force, the cracks keep expanding and the particle rotation arc keeps changing. The particles with larger rotational arcs are consistent with the location of crack distribution, and the cumulative number of cracks on the joints of high-strength rock is higher. (v) The total input energy and dissipation energy increase continuously with the shear, and the elastic energy tends to increase at the beginning of shear and then starts to decrease and gradually tends to be constant near the peak of shear stress. The total input energy and dissipation energy of the joints of the high-strength rock are larger, while the peak elastic energy of it is smaller.

1. Introduction

As a universal discontinuous medium, rock masses contain various discontinuous surfaces such as fractures, joints, weak surfaces, and faults inside [1–3], which destroy the integrity of rock masses and lead to a significant reduction in their strength and stability. Numerous engineering practices have shown that shear deformation and slip of joints can lead to engineering instability problems, which seriously threaten the safety of people's lives and properties [4]. Therefore, the in-depth study of shear characteristics of rock joints is of great significance for engineering disaster prevention and control.

Since the 1860s, scholars at home and abroad have conducted a lot of researches on the shear properties of joints through indoor tests, theoretical analysis, and numerical simulations. Quite a number of research results have been obtained, mainly including the relationships between shear strength [5–8], surface damage characteristics [9–13], shear strength and surface morphology [14–16], and the influence pattern of rock type [17], boundary conditions [18–22], and loading methods [23, 24] and other factors on them. Since Patton [25] analyzed the influence of rock joint morphology on its shear mechanical behavior, the relationship between shear properties of rock joints and joint morphology has been a hot topic of research in the rock mechanics

community in the past decades. Barton and Choubey [26] conducted a large number of experiments and summarized 10 JRC curves to predict the shear strength of joints. After that, many new methods have been proposed for the calculation of JRC [27–29]. Jiang et al. [22] developed an experimental system capable of constant normal stiffness loading (CNS) boundary conditions to compare and analyze the shear properties of rough joints under different boundary conditions. Liu et al. [30] further investigated the anisotropy of the shear properties of rough joints under different boundary conditions on this basis. With the rapid development of computer technology in recent years, numerical simulation methods have been widely used in engineering [31] and indoor experimental [20, 21] researches. Wang et al. [20] used PFC numerical simulation software to simulate the shearing process of rough joints under CNL and CNS boundary conditions and explored the damage process and the damage mechanism of rough joints under different boundary conditions from macroscopic and fine view perspectives, respectively. Zhang et al. [21] investigated the mechanism of shear deformation, damage, and energy dissipation of joints under CNL boundary conditions by indoor tests and PFC numerical simulations. Liu et al. [32, 33] also investigated the macroscopic and microscopic shear properties of through-shaped serrated joints containing first- and second-order rough bodies using a combination of indoor experiments and PFC numerical simulations. Ge et al. [34] investigated the evolution of joint roughness under CNL boundary conditions using indoor experiments and discrete element- (DEM-) based numerical simulations. Park and Song [35] used PFC^{3D} to simulate a series of joint direct shear experiments to investigate the effects of the geometrical features, and the microproperties of joints on its shear behavior were examined. Chen et al. [36] used PFC^{2D} to numerically calculate a series of nonpenetrating horizontal rock-like joints with different scales to investigate the size effect of shear mechanical properties of nonpenetrating horizontal rock-like joints. Zhang et al. [37] used PFC^{2D} to study the shear mechanical properties of joints under creep conditions.

However, most of the above studies have focused on the same strength rock conditions, and the shear characteristics exhibited by the joints are necessarily different for different joint rock strengths. For this reason, some scholars have also carried out relevant studies. Meng et al. [17] conducted shear tests under CNL boundary conditions on three different rock types and analyzed the strength characteristics and acoustic emission signal characteristics of joints of different rock types, and the results showed that rock type has a significant effect on the shear characteristics of joints. Fan et al. [38] carried out shear tests and corresponding PFC^{2D} numerical simulations of soft-hard joints with different strengths of the upper and lower joint faces and established a new peak shear strength model for soft-hard joints. Liu et al. [24] considered two typical forms of soft and hard interbedded rock joints, "soft + hard" and "hard + soft + hard," and carried out indoor shear tests and PFC^{2D} numerical simulations under CNL boundary conditions to investigate the shear properties. In the above studies, the shear properties of joints under different strength rock conditions were initially explored and some useful insights were obtained. However, the different shear properties of joints of different strength rock masses have not been compared and analyzed, and corresponding macroscopic studies have not been carried out to reveal the damage evolution process and degradation mechanism of joints of different strength rock masses.

In view of the above understanding, in order to study the macroscopic and fine shear properties of the joints of rocks of different strengths, this paper first carried out indoor one-way static direct shear tests under constant normal load (CNL) conditions on the joints of rocks of two strengths to study the macroscopic shear properties of rocks of different lithologies under different roughness conditions, which revealed the shear mechanical behavior and joint damage modes of joints of rocks with different strengths, etc. Then, the particle flow simulation software PFC^{2D} was used to dynamically simulate the whole process of shear on joints of different lithologies and to study the changes of particle contact force, number of microscopic cracks, arc of particle rotation, and microscopic damage energy on joints from the microscopic perspective and to compare the macroscopic damage evolution process of joints and their degradation mechanisms. The research results have enriched the theory of shear properties of joints and are of great significance for the prevention and control of engineering disasters caused by shear slip of joints.

2. Experimental Methods

2.1. Specimen Preparation. In order to analyze the shear characteristics of different strength rock joints, two types of rock joints with different strengths are used in the test. One is the low-strength rock on both sides of the joints (low-strength rock joints), and the other is the high-strength rock on both sides of the joints (high-strength rock joints).

In order to obtain rock joint samples of different strengths, two different material ratios were determined using materials such as cement, fine sand, and water and a method of orthogonal design. The low-strength rock joint samples were prepared using materials such as white cement, fine sand, water, and water-reducing agent and in the ratio 1 : 1 : 0.3 : 0.005 [39], and the high-strength rock joint samples were prepared using materials such as grey cement, fine sand, water, and water-reducing agent and in the ratio 1 : 0.5 : 0.25 : 0.005, respectively.

Meanwhile, to study the shear characteristics of joints of different lithologies under the influence of roughness, five steel molds representing different JRC (JRC of 0~2, 4~6, 8~10, 12~14, and 16~18, respectively) were fabricated based on Barton curves and using laser cutting techniques, and smooth joint samples of two strength rock masses and joint samples corresponding to the JRC represented by the molds (200 mm × 100 mm × 100 mm) were prepared in combination with the above molds, respectively [40, 41].

2.2. Test Apparatus and Procedure. The JAW-600 rock shear seepage test system as shown in Figure 1 was used to conduct the direct shear test. This test system mainly consists of four parts: data collection and analysis system, vertical loading unit, horizontal loading unit, and its servo control system.

At the beginning of the test, a constant normal force of 1 MPa is first applied through the vertical loading unit, and then, the quasistatic shear load is applied through the horizontal loading unit at a shear rate of 0.01 mm/s after the normal stress reaches the target value. And this process continues until the end of the test. Since the shear displacement of the joint face can be considered as failure when it reaches a critical value, the critical value of the shear displacement is usually used as the basis for controlling the end of the test. In this paper, the critical value of shear displacement is 8 mm, i.e., the shear test is terminated when the shear displacement of the specimen reaches 8 mm. And the data collection and analysis system are used to record the shear stress and shear displacement values, respectively, during the whole test.

3. Results and Discussion

3.1. Characteristics of Shear Stress-Displacement Curve. In order to compare and analyze the macroscopic shear characteristics of different roughness joints under different strength rock conditions, the stress-shear displacement curves of shear obtained from shear tests on high-strength rock joints and low-strength rock joints under six different roughnesses are given in Figure 2.

From Figure 2, it can be seen that the stress-displacement curves of low-strength rock mass with different roughness of joint shear conform to the typical peak-type curve variation trend. And the shear stress-displacement curves of the joints of high-strength rock mass also conform to the typical peak variation trend when the roughness of the joints is low. However, when the roughness increases to 12~14, the shear stress gradually increases to a certain constant value with the shear test, and the strain hardening phenomenon occurs, and there is no obvious peak point, which is consistent with the strain-hardening type curve change trend. The shear displacement when the joints of low-strength rock reach the peak point is larger than that of the joints of high-strength rock. In other words, the high-strength rock is less susceptible to shear slip than the low-strength rock under the same boundary conditions, shear rate, and roughness, i.e., so it is more resistant to shear damage.

It can also be seen from Figure 2 that in the initial stage of shear, the stress-strain curve of the low-strength rock joints in shear is downwardly convex, i.e., the slope of the tangent line of the curve gradually increases, while the stress-strain curve of the high-strength rock joints in shear is upwardly convex, i.e., the slope of the tangent line of the curve gradually decreases. Because the slope of the tangent line at a point on the stress-displacement curve of shear represents the shear stiffness at that point, it can be seen from Figure 2 that the shear stiffness of the low-intensity rock surface gradually increases and the shear stiffness of the high-intensity rock surface gradually decreases in the initial stage of shear.

In the same lithology joint test, the change trend of stress-displacement curve of joint shear under different roughness is basically the same, that is, the increase of joint roughness has no obvious effect on the change trend of stress-displacement curve of joint shear of rock mass. With the increase of the roughness of the joints, the shear strength of the joints also increases significantly, and the growth rate shows an increasing trend.

3.2. Strength Characteristics. Table 1 shows the peak shear strengths of the joints of the two strengths at different roughness and the growth rates of the peak shear strengths relative to those at the previous level of roughness. Meanwhile, the peak shear strength values of the two strength rock joints at different roughness in Table 1 are fitted to obtain exponential fitting relations with fitting coefficients of 0.999 and 0.995, respectively, as shown in

$$\begin{aligned} \tau &= 3.375 + 0.013 * \mathrm{JRC}^{1.848}, \\ R^2 &= 0.999, \\ \tau &= 3.928 + 0.045 * \mathrm{JRC}^{1.498}, \\ R^2 &= 0.995. \end{aligned} \tag{1}$$

By plotting the above two fitted relational equations in a Cartesian coordinate system, two fitted relational curves can be obtained as shown in Figure 3.

As seen from Table 1 and Figure 3, the shear strength values of the joints of both strength rock masses grow in a power function relationship as the surface roughness of the joints increases, i.e., the shear strength of the joint face increases with the increase in roughness and the growth rate also increases.

Among them, the peak shear strength of the high-strength rock joints is larger than that of the low-strength rock joints as a whole, and the growth rate of the peak shear strength of the high-strength rock joints is also larger than that of the low-strength rock joints at the same roughness. This is because, with the increase of roughness, the meshing effect of high-strength rock joints is more significant compared with that of low-strength rock joints under the action of normal pressure.

As shown in Figure 4, the residual shear strength statistics of the two strength rock joints at different roughness are shown. It can be seen from the figure that the residual strength of the high-strength rock joints is larger, and the residual strength difference is the smallest when the JRC is 4~6, and the residual strength difference is the largest when the JRC is 8~10. On the whole, the difference between the residual strength of high-strength and low-strength rock joints is little when the JRC is small, and the difference between the residual strength of the two is obvious after the JRC exceeds 6. This is mainly due to the fact that the shear stress curves of high-strength rock joints and low-strength rock joints are displacement-softening type, and

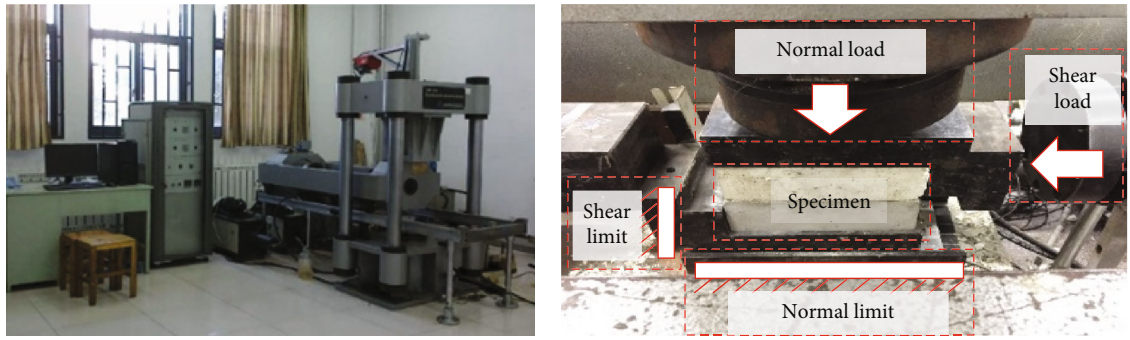

Figure 1: Arrangement of the shear test [41]: (a) shear test system; (b) loading unit.

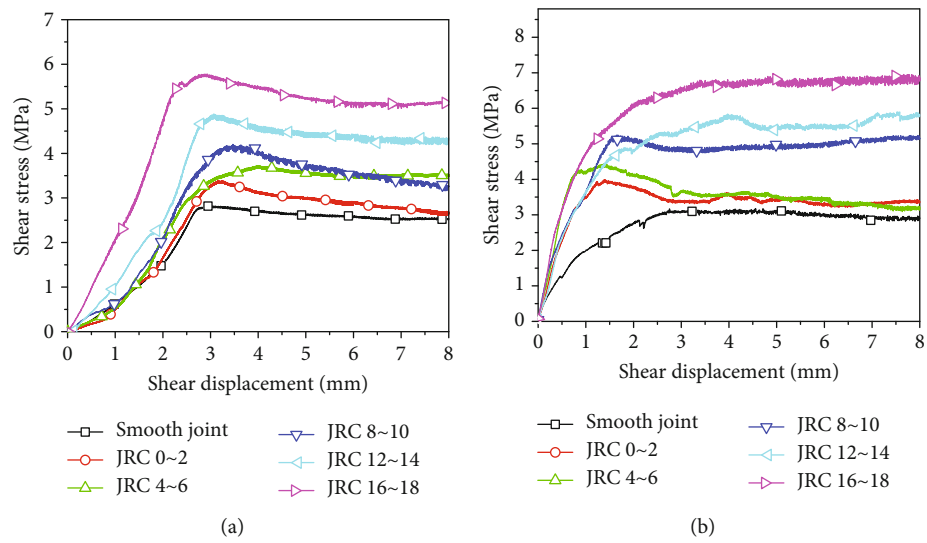

Figure 2: Curves of shear stress vs. displacement of low-strength and high-strength rock joints: (a) low-strength rock joints; (b) high-strength rock joints.

Table 1: Shear strength of joint with different lithologies.

Joint surface type	Low-strength rock mass		High-strength rock mass	
	Peak strength (MPa)	Growth rate (%)	Peak strength (MPa)	Growth rate (%)
Smooth joint	2.83		3.17	
JRC 0~2	3.38	19.43	3.98	25.56
JRC 4~6	3.72	31.45	4.43	39.75
JRC 8~10	4.20	48.41	5.34	68.45
JRC 12~14	4.88	72.44	6.02	89.91
JRC 16~18	5.78	104.24	6.97	119.87

the shear stress decreases in the residual stage as the shear proceeds, so the difference in residual strength is not large. However, when the roughness increases to 8~10, the shear stress curve of high-strength rock joints changes to strain-hardening type. As the shear proceeds, the shear stress gradually increases in the residual phase, while the shear stress of the low-strength rock joints remains strain-softening type, and the shear stress gradually decreases in the residual phase, so the difference between the two residual shear stresses is significant.

3.3. Failure Characteristics. The damage after shearing of different roughness joints of the two strength rock masses is shown in Figures 5(a) and 5(b), respectively. From the figure, it can be seen that there is no obvious damage after shear for both low-strength and high-strength rock joints when they are endowed with smooth joints. When the JRC values of the joints of the two strengths are small (low-strength joints: 0~2 and 4~6; high-strength joints: 0~2), the shear damage characteristics are mainly shown in the form of raised wear on the joints. When the JRC values of the joints of both strengths are high (low-strength rock joints: JRC > 8 ~ 10; high-strength rock faces: JRC > 4 ~ 6), the shear damage characteristics of the joints are accompanied by a large amount of shearing of the joint projections in addition to the wear of the joint projections.

A comprehensive comparison of Figures 5(a) and 5(b) shows that the shear damage characteristics of the joints of the two strength rock masses after shearing are more

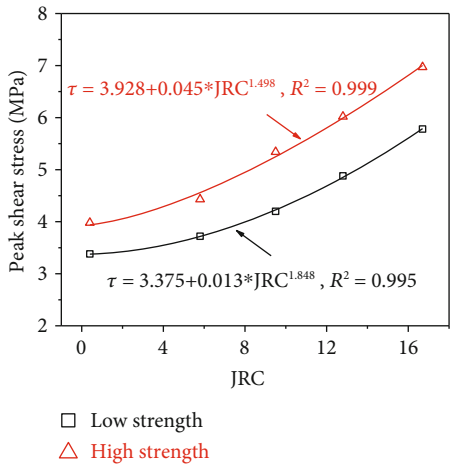

Figure 3: Relations between shear strength and JRC of joint.

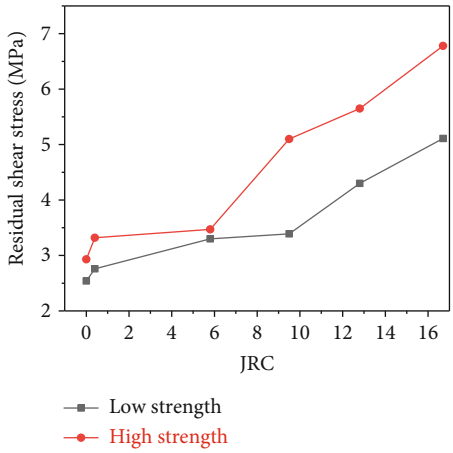

Figure 4: Residual shear strength of low-strength and high-strength rock joints with different JRC.

significant than those of the joints of the low-strength rock masses as the JRC increases, i.e., when the JRC of the joints of the two different strength rock masses are at the same level, the shear damage characteristics of the joint samples of the high-strength rock masses are more significant. This phenomenon indicates that the joints of high-strength rock still need to overcome a large frictional resistance after convex shearing and also explains the small reduction of shear stress in the postpeak phase of the shear curve of high-strength rock and the insignificant strain-softening phase.

4. Numerical Simulation of Shear Failure Mechanism

4.1. Numerical Simulation Scheme. In order to study the damage evolution process and degradation mechanism of the joints of the rock during shear, the numerical calculation model for typical working conditions (JRC of 12~14) was established by PFC^{2D} software based on the indoor tests. The dimensions of the established numerical model and the loading method are the same as those of the indoor test model. The numerical model of the rock joints was established according to the procedure shown in Figure 6. Firstly, the wall around the shear box is generated according to the specimen size, and secondly, the spheres are generated inside the wall according to the calibrated fine view parameters, and the contact model between the spheres is set to linear, as shown in Figure 6(a). Then, a certain circumferential pressure is applied to the specimen, and after the spheres are compacted, the contact model between the spheres is changed to linearpbond. The advantage of this step is to ensure that the cementation between all the spheres can be added (the pb-state is all displayed as "3"), as in Figure 6(b). After that, the joint profile is established and the spheres are grouped by importing the already drawn Barton curves, and the walls are regenerated according to the coordinates of the joint, as in Figure 6(c). The advantage of establishing the joint in this step is to ensure that the shape of the joints is the same as that of the joints of the experimental specimen and will not change during the modeling process due to the movement of the particles. In general, the joint model can be created by changing the contact properties of the particles on both sides of the joints, but due to the bump effect of the circular particles in the BPM model, the parameters of the created joints are high. Peter Cundall developed the smooth joint contact model for this purpose, which can avoid the bump effect of the particles and make the numerical simulation results more consistent with the actual results. Therefore, the contact model at the joints was changed to smooth joint, as shown in Figure 6(d).

The boundary conditions imposed in the numerical simulation are the same as those in the indoor test, limiting the horizontal displacements of wall_4 and wall_5 and the normal displacement of wall_3, controlling the vertical velocity of wall_6 by the servo function to achieve a constant normal stress (1 MPa) loading, and applying a constant horizontal velocity to wall_1, wall_2, and wall_3 (0.01 mm/s) to achieve unidirectional static shear load conditions. In PFC, the shear stress at the joint surface is derived mainly from the horizontal load between the particles and the wall, specifically: monitoring the horizontal load between the wall and the particle on the left side (wall_1 and wall_4) and the right side (wall_3 and wall_2) of the specimen, respectively, then taking the average of the left and right sides to obtain the shear load at the joint surface, and finally dividing by the joint surface length (200 mm) to get the shear stress on the joint surface. The monitoring of shear displacement is mainly achieved by monitoring the average horizontal displacement of the lower 3 sides of the specimen (wall_1, wall_2, and wall_3). After the model was established, the stress-shear displacement curves of the shear of two different strengths of the joints of the rock with JRC 12~14 at a constant normal stress of 1 MPa were used as calibration benchmarks to compare the simulation and indoor test results, and the numerical model was repeatedly calibrated using the "trial and error method" for the microscopic mechanical parameters [42]. The final obtained microscopic mechanical parameters are shown in Tables 2 and 3. The stress-shear displacement comparison curves of the numerical simulation and the shear of the indoor test are shown in Figure 7.

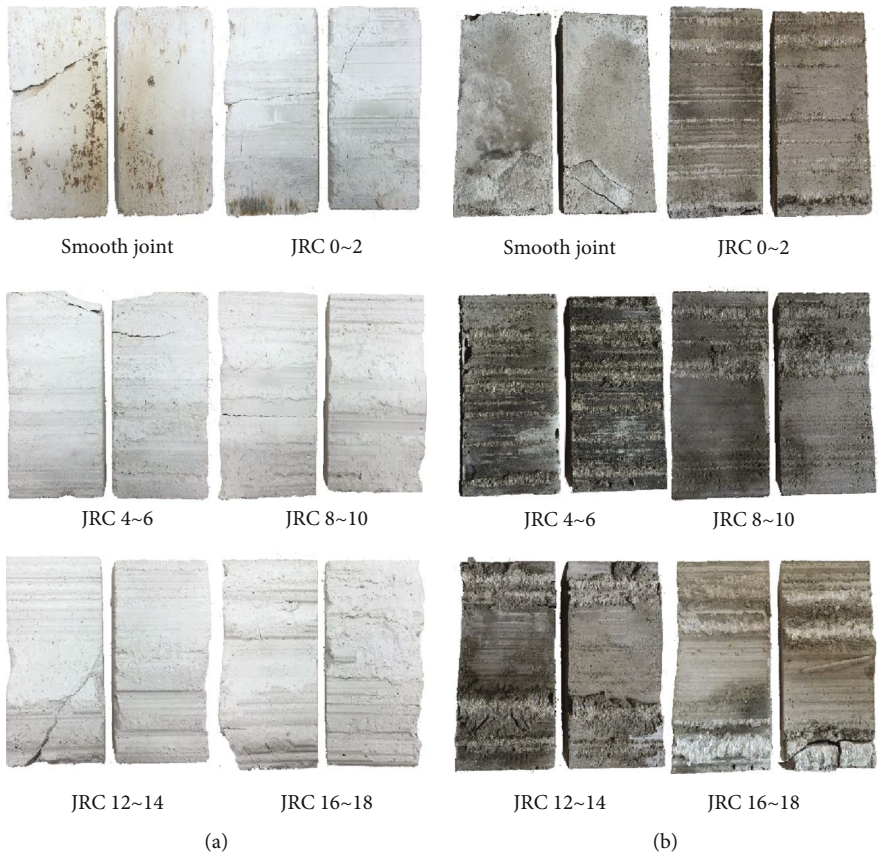

Figure 5: Shear failure model of low-strength rock joints and high-strength rock joints: (a) low-strength rock joint; (b) high-strength rock joints.

4.2. Cracking Process and Contact Force Evolution

4.2.1. Analysis of Interparticle Contact Force Evolution. During the shearing process of the rock mass, the upper and lower rock masses will be shear misaligned with each other, which makes the contact characteristics between the granules change continuously, and in turn, the contact force between the granules will also change continuously. Figure 8 shows the distribution and size evolution of the contact force detected at different shear displacements (1, 2, 3, 4, 5, 6, 7, and 8 mm) inside the rock mass, where different colors represent different contact forces. And the larger the contact force, the thicker the line. The larger the contact force between the particles, the more intense the extrusion between the particles, i.e., the size distribution of the interparticle contact force reflects the extrusion between the internal particles in the joints of the rock.

As shown in Figures 8(a) and 8(b), the distribution of contact force magnitudes between particles inside the rock during shearing of high-strength joint rocks and low-strength joint rocks is shown. As can be seen from the figures, the magnitude and orientation of the contact forces between the particles are changing as shearing proceeds. From the overall point of view, the contact force is larger at the projection of the joints during shear, and the contact force inside the rock is smaller. Generally, the joint roughness can be divided into first-order asperities (waviness) and second-order asperities (unevenness), and the two types of roughness jointly exert shear resistance during shear [25, 43]. In the early stage of shear, the contact forces on the structure surface are mainly concentrated on a few points, which are second-order rough bumps on the structure surface. As the shear proceeds, the contact force on these points gradually increases, causing the damage to this part of the projection to occur. Due to the destruction of the second-order bumps on the surface of the joints, the joint contact begins to redistribute and the points with higher contact forces begin to shift. With the further increase of shear displacement, the joint contact force is gradually concentrated to one place, i.e., the first-order rough bump.

Comparing Figures 8(a) and 8(b), it can be found that the joint contact force is greater for high-strength joint rocks under the same shear displacement conditions, and the contact force is concentrated on the first-order roughness within a smaller shear displacement. This indicates that the higher the force on the second-order roughness of the joints under the same conditions of the high-strength joint rock, the earlier and more serious the damage of the joint projection occurs. And it can also be found from the figure that the joint contact force is more widely distributed and the value is larger in the postpeak phase for high-strength joint rocks compared to low-strength joint rocks, which also explains why the shear stress curve of high-strength joint rocks is hardened while the shear curve of low-strength joint rocks is softened.

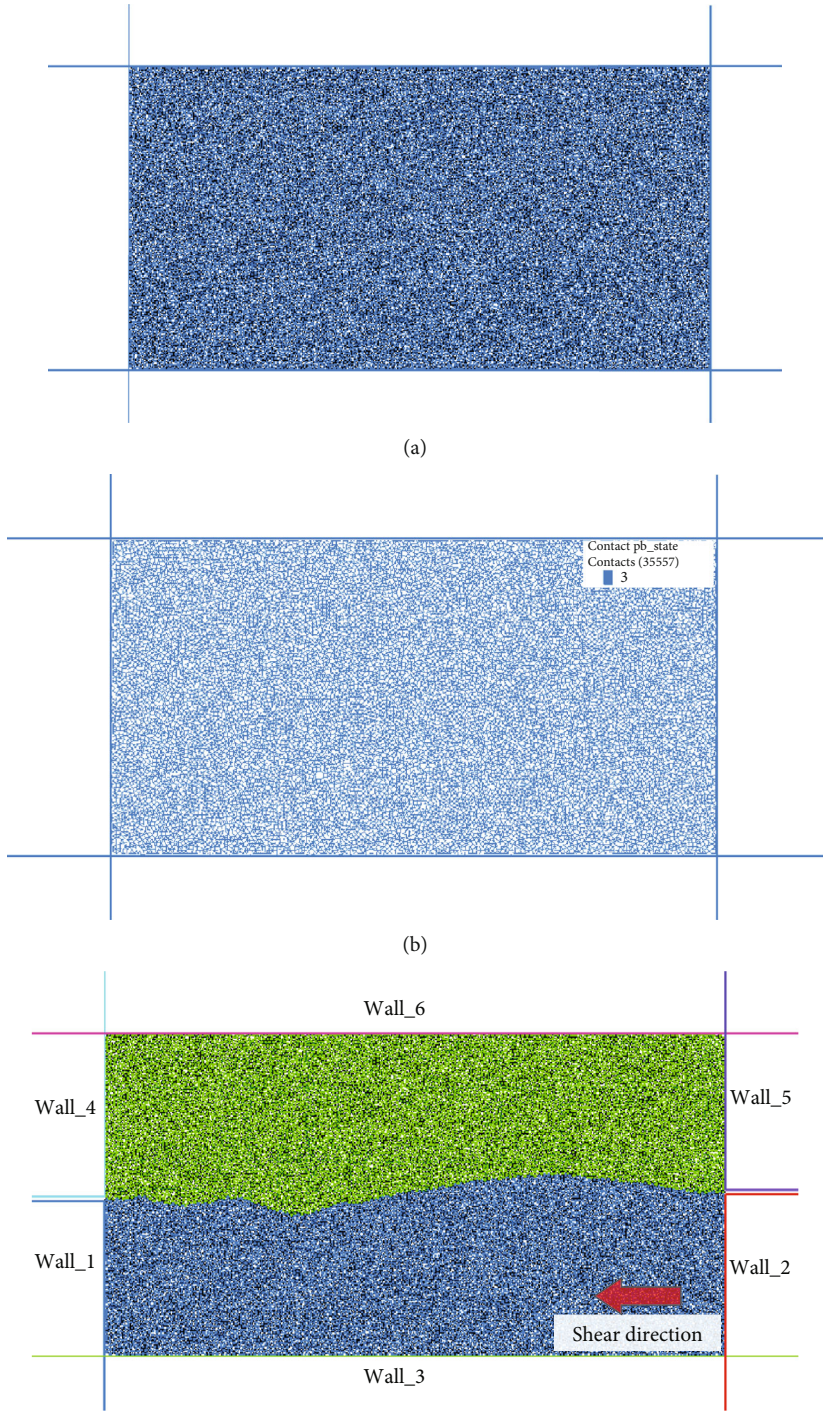

Figure 6: Continued.

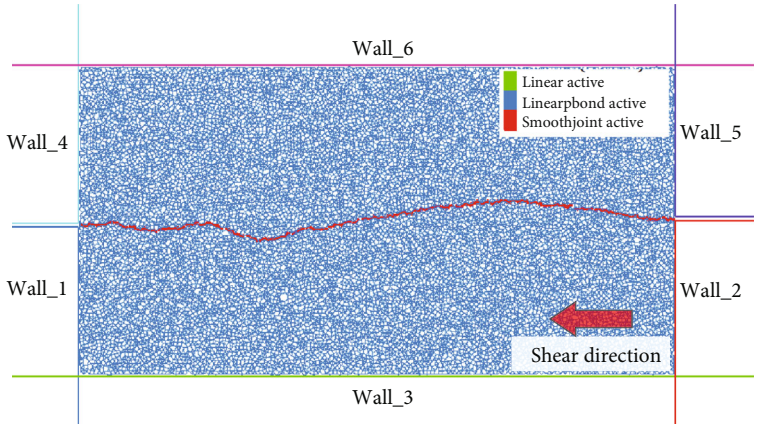

(d)

Figure 6: Construction process of anisotropic structure surface shear numerical model: (a) generation of particles; (b) change of contact model; (c) adding joints; (d) changing the joint contact model.

Table 2: Numerical calculation of microscopic mechanical parameters of low-strength rock joint.

Particle parameters	Value	Parallel bond parameters	Value	Smooth joint properties	Value
Young's modulus (GPa)	7.5	Young's modulus (GPa)	7.5	Normal stiffness (MPa/mm)	57
Ratio of normal to shear stiffness	1.0	Ratio of normal to shear stiffness	1.0	Tangential stiffness (MPa/mm)	14
Minimum particle radius (mm)	0.5	Normal strength (MPa)	31 ± 3.1	Friction coefficient	0.75
Radius ratio	1.66	Shear strength (MPa)	40 ± 4.1	Bond shear strength (MPa)	0
Density (kg/m^3)	2300			Bond normal strength (MPa)	0
Friction coefficient	0.5				

Table 3: Numerical calculation of microscopic mechanical parameters of high-strength rock joint.

Particle parameters	Value	Parallel bond parameters	Value	Smooth joint properties	Value
Young's modulus (GPa)	14	Young's modulus (GPa)	14	Normal stiffness (MPa/mm)	80
Ratio of normal to shear stiffness	1.5	Ratio of normal to shear stiffness	1.5	Tangential stiffness (MPa/mm)	80
Minimum particle radius (mm)	0.5	Normal strength (MPa)	41 ± 4.1	Friction coefficient	0.85
Radius ratio	1.66	Shear strength (MPa)	52 ± 5.1	Bond shear strength (MPa)	0
Density (kg/m^3)	2750			Bond normal strength (MPa)	0
Friction coefficient	0.6				

4.2.2. Analysis of Crack Growth Evolution. Figure 9 shows the numerical simulation evolution of the crack distribution inside the rock mass under different shear displacements in the shear process for the two strength rock joints. From the figure, it can be obtained that the crack development process of the two strength joints is similar. In order to better analyze the crack development law of the two strength joints, the number of cracks generated per unit time and the accumulated number of cracks in the joints during shear are counted, as shown in Figure 10. As can be seen from Figures 9 and 10, in the initial stage of shear (stage I), only a small number of cracks are generated at this stage because most of the interparticle contacts are in the linear elastic stage. After the elastic stage, the stress reaches the yield point and the specimen enters the stable rupture propagation stage, where the number of cracks starts to increase slowly and reaches the peak number of cracks at the peak shear stress. After the shear stress exceeds the peak point (stage II), the specimen enters the postpeak stage, and the number of cracks at this stage starts to gradually decrease and fluctuate, which is due to a large number of bumps on the joints being sheared and crushed, and the specimen shifts from the stable rupture propagation stage to the unstable rupture propagation stage, where the number of cracks fluctuates and penetrates the entire joints. Until entering stage III, the number of cracks tends to develop smoothly in general and is at a lower level, which is due to the fact that after the second-order roughness of the joints is sheared and crushed, the stress is gradually concentrated in the first-order roughness, and compared with the second-order

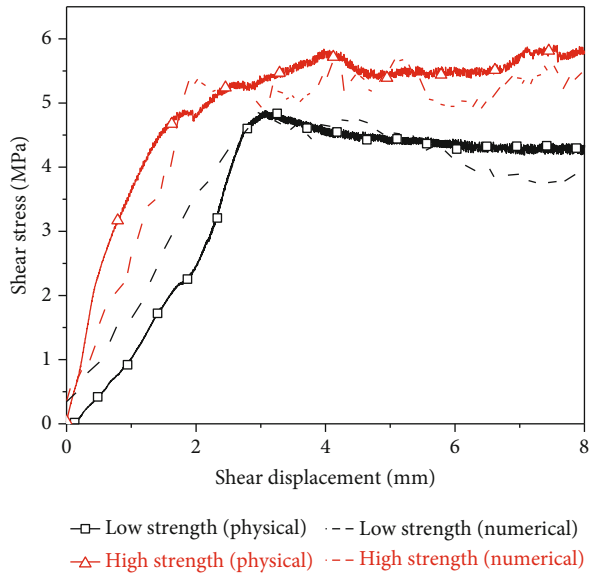

Figure 7: Shear stress-shear displacement curves of shear of indoor experiments and numerical simulations.

roughness, the first-order roughness is less prone to violent damage, and the joint resumes the development trend of stable rupture.

Comparing the crack development diagrams of joints of different lithologies, it can also be seen that the higher the strength of the joints, the earlier the maximum number of cracks in the joints appears and the larger the cumulative number of cracks. That is, it indicates that the damage of the joints becomes more serious at an earlier stage, which is consistent with the phenomenon observed in the indoor tests.

It can also be seen from Figure 9 that the number of tension cracks in the shear process is greater than the number of shear cracks, which is due to the fact that the internal contact force is dominated by pressure during the shear process on the joints of the rock, making the mutual extrusion between the particles resulting in the development of cracks mainly in tension cracks.

4.2.3. Analysis of Particle Rotation Radian Evolution. Figure 11 shows the evolution of the particle rotation arc inside the joints of the two strength rock masses when monitoring different shear displacements. From Figures 11(a) and 11(b), it can be seen that the shear misalignment of the rock mass causes the change of the internal rotational arc of the particle system, which in turn leads to the gradual evolution of the rotational arc of the particle body. In the initial stage of shear, the rotational arc of the particle body inside the rock mass is at a small level, and most of the particle rotational arcs are between -1 and 0, and only individual particles have slightly larger rotational arcs. Under the action of shear load, the compression density at the end of the rock body causes the particle body to rotate, so the rotation arc of the particles on the side of the applied shear stress (right side of the lower specimen) and the fixed side of the upper specimen (left side of the upper specimen) increases, and the rotation arc of the particles is mainly between 0 and 0.5. When the shear displacement further increases, the more particles with rotation arcs of 0 to 0.5 are gradually expanded from the two ends of the specimen to the lower left and upper right ends of the rock mass. The particles with high rotational arcs (i.e., rotational arcs of -600 to -1 and 1 to 600) are mainly distributed at the projections of the joint. And compared with the crack distribution, it can be found that these particles with high rotational arcs are mainly concentrated at the locations where cracks are generated. This is mainly the shear process in which the joint projection is the main bearing area. It is subjected to large normal stress and shear stress, so the granular body in this region is moving vigorously, accumulating more energy, and the rock is more prone to damage. It can be seen that the generation of cracks is related to the rotation of the particles, and the process of rock destruction is also a continuous redistribution of the internal particle rotation arc. Along with the continuous generation of cracks, it leads to the evolution of the rock mass from microscopic rupture to macroscopic failure.

To further analyze the evolution law of particle rotation arc during shearing, the proportion of the number of particles with particle rotation arcs of -600~-1, -1~0, 0~0.5, 0.5~1, and 1~600 was counted, as shown in Figure 11(c). As can be seen from the figure, the evolution process of particle rotational arcs on the joints of the two strength rock masses is roughly similar. Among them, particles with rotational arcs of 0.5~0 and 0~-1 account for the largest proportion. With the increase of shear displacement, the number of particles with rotational arcs of -1~0 shows an overall decreasing trend. In the initial stage of shear, the percentage changes less and tends to be smooth overall, while after the peak shear stress, the percentage decreases rapidly from 75% to about 50%. And after the shear displacement to 6 mm, the percentage tends to be smooth again roughly stabilized at about 50%. The proportion of particles with a rotational arc of 0.5 to 0 is on the whole on an upward trend from 20% to about 40%, and the growth trend of this proportion of particles is the opposite of the decreasing trend of the proportion of particles from -1 to 0. The percentage of particles with rotational arcs of 1~600, -1~-600, and 0.5~1 all show an increasing trend basically from 0% to about 3% slowly. Comparing the histograms of the joints of the two intensities, it is also clear that the decrease in the percentage of particles with rotational arcs of 0~-1 on the joints of the low-intensity rock is more continuous, while the joints of the high-intensity rock show a stepwise pattern, which is related to the damage pattern and range of the joints.

4.3. Evolution Characteristics of Energy

4.3.1. Determination of Dissipation Energy. The physical and mechanical change processes of rock are closely related to energy transformation, and its deformation and failure are instability phenomena driven by energy exchange [44].

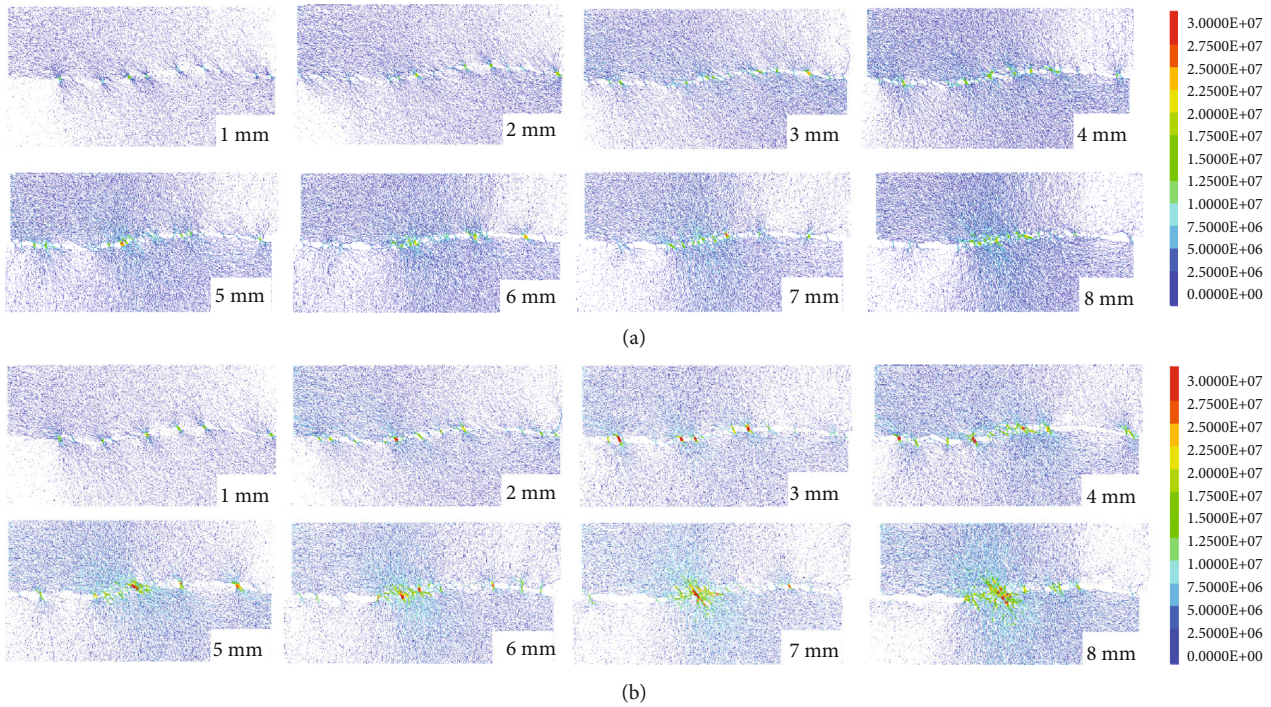

Figure 8: Evolution of contact force between particles during shearing: (a) low-strength rock joints; (b) high-strength rock joints.

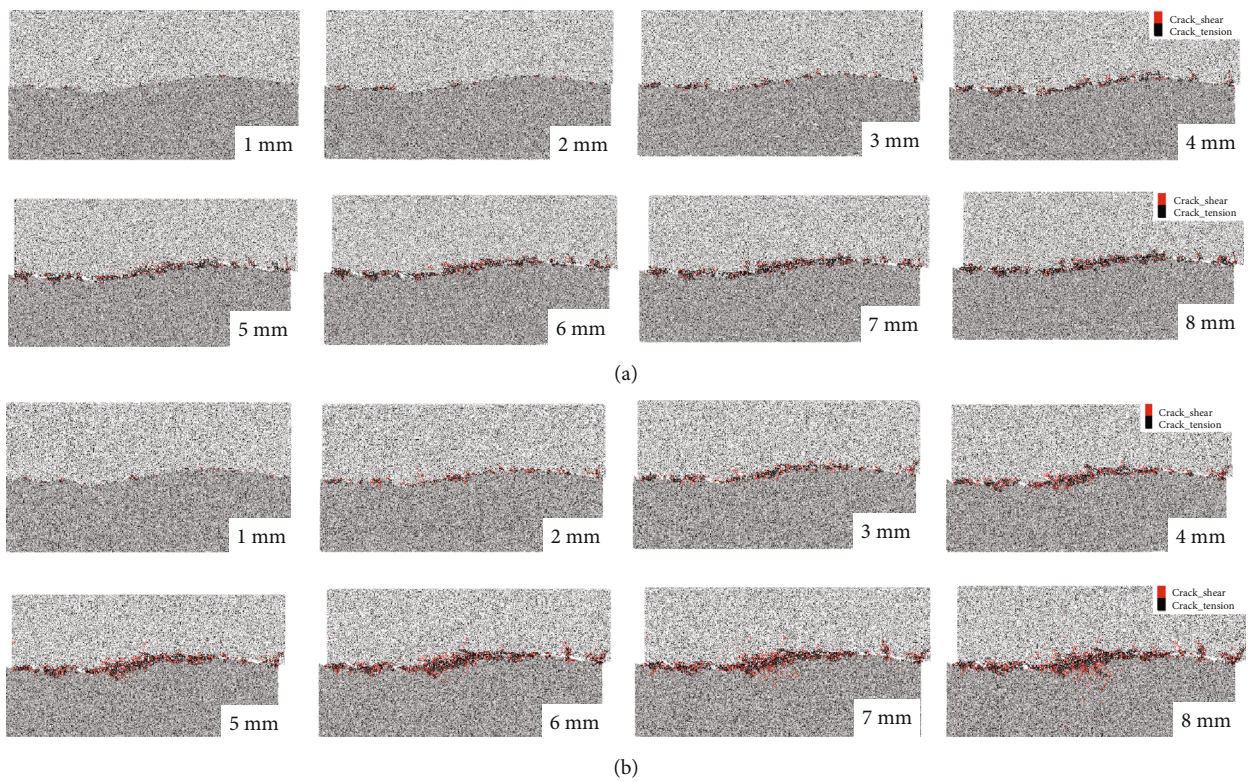

Figure 9: Evolution of microcracks during shearing: (a) low-strength rock joints; (b) high-strength rock joints.

Therefore, the energy dissipation can reflect the damage of the specimen, and the analysis of the energy evolution process of the joint of the rock body can also reveal the damage mechanism of the joint.

According to the law of energy conservation, the expression of total external energy U is as follows:

$$U = U_e + U_d + U_k, \tag{2}$$

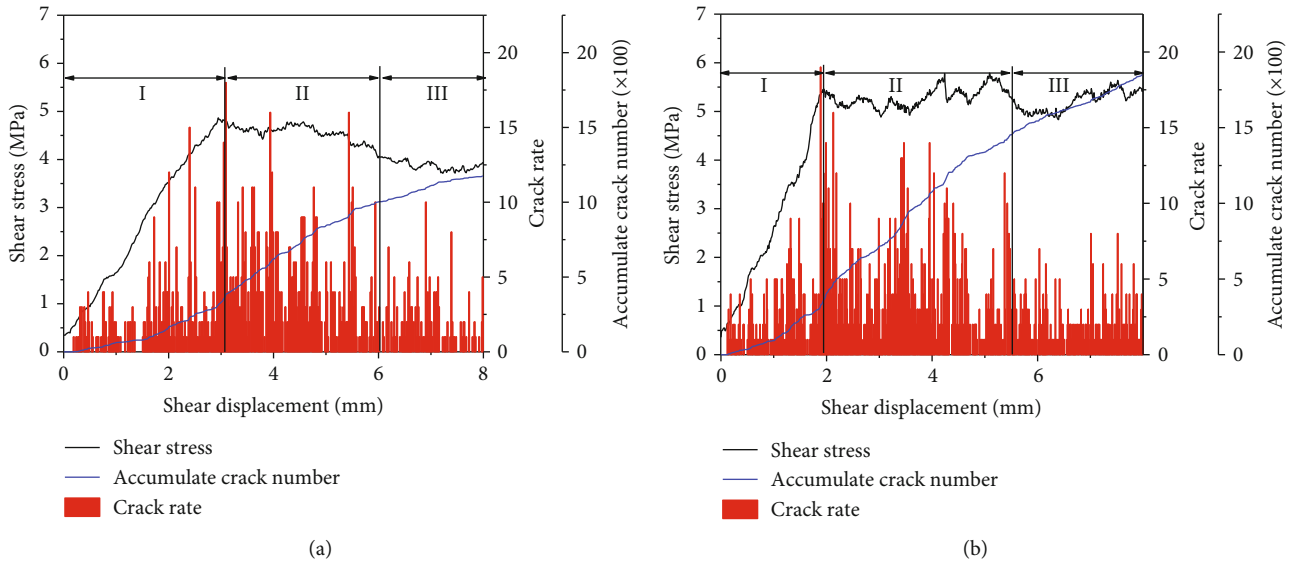

Figure 10: Number of cracks and cumulative number of cracks: (a) low-strength rock joints; (b) high-strength rock joints.

where U_e is the elastic energy, U_d is the dissipative energy, and U_k is the kinetic energy.

Since the shear speed is 0.01 mm/s during the whole simulated shear process, the kinetic energy is negligible, so the total energy expression can be simplified as

$$U = U_e + U_d. \tag{3}$$

In the PFC numerical simulation software, the total external input energy is Wall's boundary energy E_z. The elastic energy is mainly the linear elastic energy E_s and the gluing elastic energy E_b, as shown in the following:

$$U_e = E_s + E_b. \tag{4}$$

Among them, Wall's boundary energy E_z, linear elastic energy E_s, and gluing elastic energy E_b can be calculated by the self-contained function of the PFC numerical simulation software [45]; the equations are as follows:

$$\begin{aligned} E_z &= \sum_{N_w} (F_i d_i), \\ E_s &= \frac{1}{2}\left(\frac{(F_n^l)^2}{k_n} + \frac{\|F_s^l\|^2}{k_s}\right), \\ E_b &= \frac{1}{2}\left(\frac{F_n^2}{k_n A} + \frac{\|F_s\|^2}{k_s A} + \frac{\|M_b\|^2}{k_n I}\right), \end{aligned} \tag{5}$$

where N_w is the number of walls; F_i is the force exerted on the wall; d_i is the displacement of the wall; F_n^l is the linear normal force; F_s^l is the linear shear force; k_n is the linear normal stiffness; k_s is the linear shear stiffness. A is the cross-sectional area; I is the moment of inertia of the parallel bond cross-section; F_n is the normal force of parallel bond; F_s is the shear force of parallel bond; k_n and k_s are the normal and shear stiffness of parallel bond; M_b is the moment of parallel bond.

Dissipative energy is mainly generated by friction, damping dissipation, microrupture, and plastic deformation and can be obtained by subtracting the elastic energy from the total external energy, i.e.,

$$U_d = U - U_e. \tag{6}$$

4.3.2. Energy Evolution. As shown in Figure 12, the curves of the total external input energy, elastic energy, and dissipation energy changes during shear for the high-strength rock joints and low-strength rock joints are shown. As a whole, the energy evolution process of high-strength rock joints and low-intensity rock joints is similar. In the preshear stage, i.e., stage I, the total input energy increases rapidly with the increase of shear stress, shear displacement, and normal displacement. As the connection and cementation of most of the particles in the early stage of shear are still in the elastic stage, the elastic energy accumulates continuously as the shear proceeds. However, the analysis above shows that a small amount of cracks are generated in this stage and there is some damage, so some dissipation energy is also generated in this stage. And the dissipation energy is first at a small level and then starts to rise slowly. After the shear displacement exceeds a certain range, the rising rate increases rapidly, which is the same as the trend of the number of cracks accumulated on the joints during shear. The elastic energy reaches its peak by the time it reaches the peak of the shear stress, after which macroscopic damage occurs in stage II due to a large number of cracks on the joints. The elastic energy stored between the particle joints and between the glue junctions is consumed, causing the elastic energy curve to start decreasing. And the dissipation energy still keeps growing at a large rate. In stage III, the elastic energy remains basically the same, while the dissipation energy continues to increase. This is due to the fact that there are still a

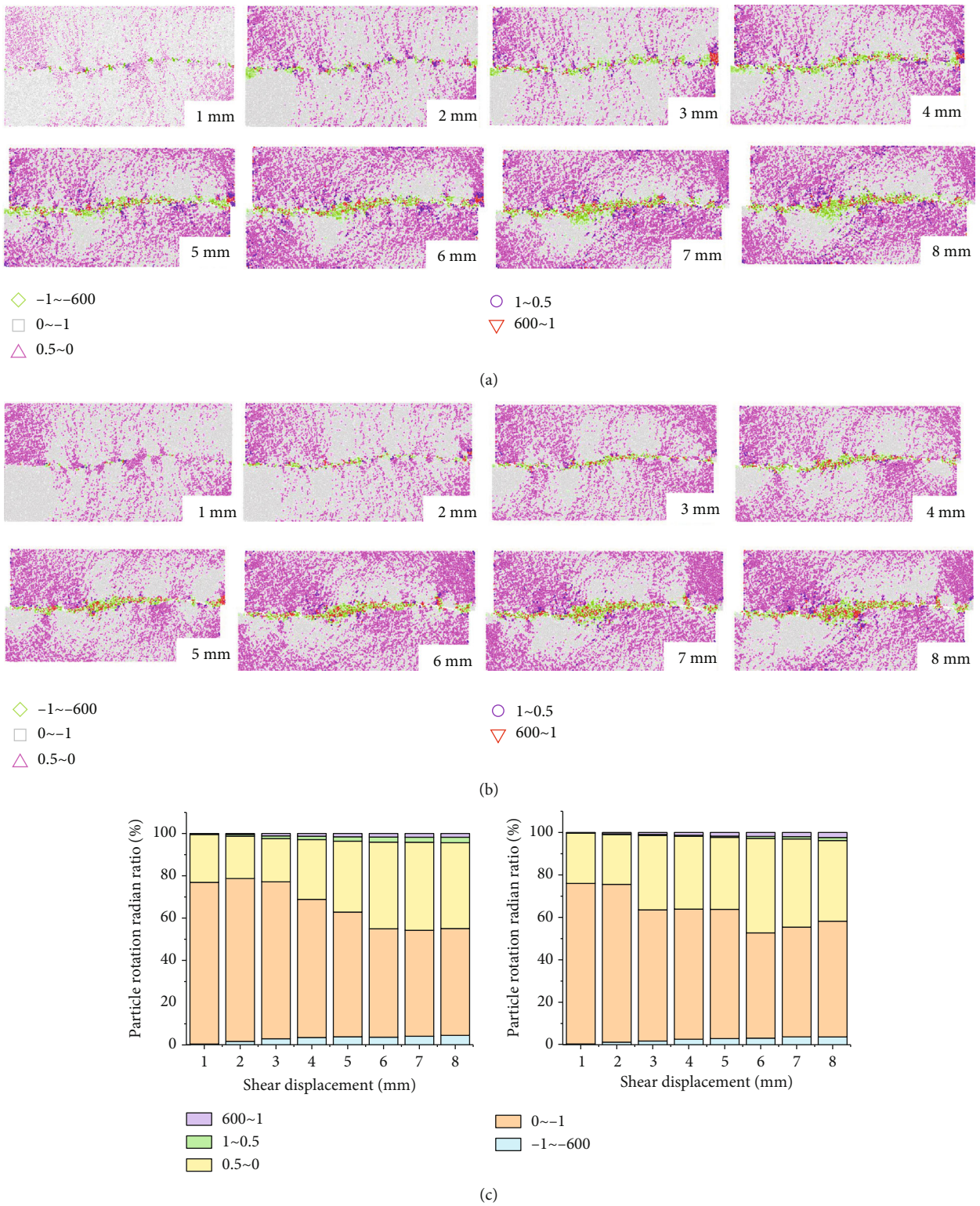

Figure 11: Evolution of particle rotation radian during shearing: (a) low-strength rock joints; (b) high-strength rock joints; (c) the percentage of particle rotation arc.

large number of cracks generated in this stage and the friction between particle contacts increases, so the frictional dissipation energy becomes the main energy dissipated.

Comparing the energy evolution curves of high-strength joint rocks and low-strength joint rocks, it can be seen that the high-strength joint rocks have greater total input energy,

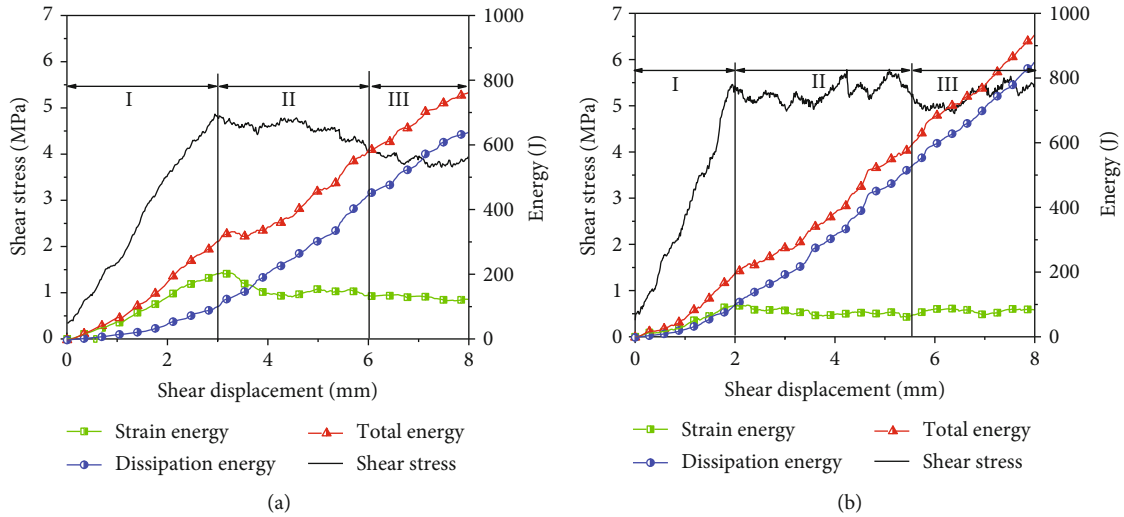

Figure 12: Variation curve of energy with shear displacement: (a) low-strength rock joints; (b) high-strength rock joints.

greater dissipation energy, and smaller peak elastic energy. This is due to the fact that the high-strength joint rock specimens have higher input shear stress and higher normal displacement during shear, which in turn results in higher total input energy. As shown in the above analysis, under the same conditions, the joint projections of high-strength joint rocks are damaged earlier and more severely than those of low-strength joint rocks, and a large number of cracks are produced at a smaller shear displacement. Therefore, the accumulated elastic energy is smaller, while the dissipation energy is larger.

5. Conclusion

In order to study the effect of rock mass strength on the macroscopic and microscopic shear properties of the joints, shear tests of rock specimens of two strengths were conducted in the laboratory and corresponding numerical simulations were carried out using PFC^{2D} numerical simulation software, and then, a systematic study of the shear properties of the joints of rock masses of different strengths was carried out from the macroscopic and microscopic perspectives, and the following conclusions were obtained:

(1) The shear stress curves of rock masses with different strengths tend to be different. High-strength rock masses tend to be hardened and low-strength rock masses tend to be softened. And comparing the test results under multiple roughness conditions, we can also find that the joints of high-strength rock masses are more sensitive to the change of roughness

(2) With the increase of JRC, the surface damage mode of the joints of both strength rock masses gradually changes from "abrasion" to "abrasion + gnawing". The damage range of high-strength joints is larger, which means that the high-strength joints are less susceptible to shear slip than the low-strength rock mass surface

(3) In the simulated shear process, the contact force is mainly concentrated on the joints, while the contact force inside the rock is smaller. And the contact force on the joints first acts on the second-order roughness and then gradually acts on the first-order roughness. Compared with the low-strength rock masses, the contact force on the joints of the high-strength rock masses is larger and more widely distributed

(4) At the early stage of shear, more rotations occurred in the end particle body, and only a small number of cracks occurred on the joints. With the increase of shear displacement, the number of particles and cracks with larger rotational arc increases rapidly, and the particle arc is mainly concentrated in the location where cracks occur. The cumulative number of cracks on the joints of the high-strength rock masses is more, and the particles with larger rotational arcs are distributed more widely

(5) As shearing proceeds, the total input energy continues to increase. At the beginning of shear, the elastic energy is greater than the dissipative energy. Near the peak of shear, the elastic energy reaches its peak and then begins to decrease and gradually tends to be constant. However, the dissipative energy keeps increasing and eventually becomes much larger than the elastic energy. The input energy and dissipation energy of the high-strength joint rock specimens are greater, while the peak elastic energy is smaller

Data Availability

The data used to support the findings of this study are available from the corresponding author upon request.

Conflicts of Interest

The authors declare no conflict of interest.

Acknowledgments

This work is supported by the National Natural Science Foundation of China (No. 52104093) and the Shandong Provincial Natural Science Foundation (Nos. ZR2019BEE065 and ZR2020QE120).

References

[1] Y. Su, F. Y. Zang, Y. Q. Li, Y. Q. Du, and W. Y. Wang, "Shear failure mode of anchored rock mass with through joints," *The Chinese Journal of Geological Hazard and Control*, vol. 31, no. 5, pp. 133–140, 2020.

[2] L. D. Wang, B. Y. Hao, and M. X. Liang, "Slurry diffusion of single fracture based on fluid-solid coupling," *Journal of Mining and Strata Control Engineering*, vol. 3, no. 1, pp. 104–112, 2021.

[3] J. K. Li and H. Wang, "Ground support of interbedded rock roof in a deep roadway with fully-anchored cables," *Journal of Mining and Strata Control Engineering*, vol. 2, no. 3, pp. 14–22, 2020.

[4] X. B. Yang, J. Zhou, Y. M. Song, and X. X. Han, "Evolution characteristics of sliding displacement of rock interface under cyclic loading," *Journal of China Coal Society*, vol. 44, no. 10, pp. 3041–3048, 2019.

[5] N. Barton, "The shear strength of rock and rock joints," *International Journal of Rock Mechanics and Mining Sciences & Geomechanics Abstracts*, vol. 13, no. 9, pp. 255–279, 1976.

[6] N. Barton, S. Bandis, and K. Bakhtar, "Strength, deformation and conductivity coupling of rock joints," *International Journal of Rock Mechanics and Mining Sciences & Geomechanics Abstracts*, vol. 22, no. 3, pp. 121–140, 1985.

[7] C. C. Xia, Z. C. Tang, W. M. Xiao, and Y. L. Song, "New peak shear strength criterion of rock joints based on quantified surface description," *Rock Mechanics and Rock Engineering*, vol. 47, no. 2, pp. 387–400, 2014.

[8] J. Yang, G. Rong, D. Hou, J. Peng, and C. B. Zhou, "Experimental study on peak shear strength criterion for rock joints," *Rock Mechanics and Rock Engineering*, vol. 49, no. 3, pp. 821–835, 2016.

[9] A. Karami and D. Stead, "Asperity degradation and damage in the direct shear test: a hybrid fem/dem approach," *Rock Mechanics and Rock Engineering*, vol. 41, no. 2, pp. 229–266, 2008.

[10] M. S. Asadi, V. Rasouli, and G. Barla, "A laboratory shear cell used for simulation of shear strength and asperity degradation of rough rock fractures," *Rock Mechanics and Rock Engineering*, vol. 46, no. 4, pp. 683–699, 2013.

[11] M. Bahaaddini, P. C. Hagan, R. Mitra, and M. H. Khosravi, "Experimental and numerical study of asperity degradation in the direct shear test," *Engineering Geology*, vol. 204, pp. 41–52, 2016.

[12] Z. H. Zhao, H. Peng, W. Wu, and Y. F. Chen, "Characteristics of shear-induced asperity degradation of rock fractures and implications for solute retardation," *International Journal of Rock Mechanics and Mining Sciences*, vol. 105, pp. 53–61, 2018.

[13] F. Z. Meng, H. Zhou, Z. Q. Wang et al., "Characteristics of asperity damage and its influence on the shear behavior of granite joints," *Rock Mechanics and Rock Engineering*, vol. 51, no. 2, pp. 429–449, 2018.

[14] G. Grasselli, "Shear strength of rock joints based on quantified surface description," At the Civil Engineering Department, EPF Lausanne, Switzerland, 2001.

[15] A. Fathi, Z. Moradian, P. Rivard, G. Ballivy, and A. J. Boyd, "Geometric effect of asperities on shear mechanism of rock joints," *Rock Mechanics and Rock Engineering*, vol. 49, no. 3, pp. 801–820, 2016.

[16] W. M. Xiao, C. C. Xia, W. Wang, S. G. Du, and R. G. Deng, "Contact algorithm for determining aperture evolution of rock fracture during shearing," *International Journal of Geomechanics*, vol. 16, no. 2, pp. 1–13, 2016.

[17] F. Z. Meng, H. Zhou, S. J. Li et al., "Shear behaviour and acoustic emission characteristics of different joints under various stress levels," *Rock Mechanics and Rock Engineering*, vol. 49, no. 12, pp. 4919–4928, 2016.

[18] G. J. Cui, C. Q. Zhang, H. C. Han, Z. Q. Zeng, H. Zhou, and J. J. Lu, "Experiment study on shear behavior of artificial joint under CNL and CNS boundary conditions," *Chinese Journal of Rock Mechanics and Engineering*, vol. 38, no. S2, pp. 3384–3392, 2019.

[19] Q. Yin, H. W. Jing, B. Meng, R. C. Liu, Y. J. Wu, and Y. J. Wu, "Macroscopic and microscopic shear mechanical properties of sandstone under CNL and CNS boundary conditions," *Journal of Mining & Safety Engineering*, vol. 38, no. 3, pp. 615–624, 2020.

[20] G. Wang, X. P. Zhang, Y. J. Jiang, B. Li, X. Z. Wu, and N. Huang, "Meso-mechanism research on shear failure of rock joint based on particle discrete element method," *Journal of Central South University*, vol. 46, no. 4, pp. 1442–1453, 2015.

[21] X. P. Zhang, Y. J. Jiang, G. Wang et al., "Mechanism of shear deformation, failure and energy dissipation of artificial rock joint in terms of physical and numerical consideration," *Geosciences Journal*, vol. 23, no. 3, pp. 519–529, 2019.

[22] Y. Jiang, J. Xiao, Y. Tanabashi, and T. Mizokami, "Development of an automated servo-controlled direct shear apparatus applying a constant normal stiffness condition," *International Journal of Rock Mechanics and Mining Sciences*, vol. 41, no. 2, pp. 275–286, 2004.

[23] W. C. Fan, P. Cao, and L. Long, "Degradation of joint surface morphology, shear behavior and closure characteristics during cyclic loading," *Journal of Central South University*, vol. 25, no. 3, pp. 653–661, 2018.

[24] X. R. Liu, B. Xu, X. H. Zhou, L. Yi, X. Zeng, and J. W. Wang, "Investigation on the macro-meso shear mechanical properties of soft-hard interbedded rock discontinuity," *Journal of China Coal Society*, vol. 40, no. 9, pp. 2895–2909, 2021.

[25] F. D. Patton, "Multiple modes of shear failure in rock," in *Proceedings of the 1st Congress of the International Society of Rock Mechanics*, pp. 509–513, Lisbon, Portugal, 1966.

[26] N. Barton and V. Choubey, "The shear strength of rock joints in theory and practice," *Rock Mechanics*, vol. 10, no. 1-2, pp. 1–54, 1977.

[27] G. C. Zhang, M. Karakus, H. M. Tang, Y. F. Ge, and L. Zhang, "A new method estimating the 2D joint roughness coefficient for discontinuity surfaces in rock masses," *International Journal of Rock Mechanics and Mining Sciences*, vol. 72, pp. 191–198, 2014.

[28] R. Tse and D. M. Cruden, "Estimating joint roughness coefficients," *International Journal of Rock Mechanics and Mining Sciences & Geomechanics Abstracts*, vol. 16, no. 5, pp. 303–307, 1979.

[29] Y. F. Ge, P. H. S. W. Kulatilake, H. Tang, and C. G. Xiong, "Investigation of natural rock joint roughness," *Computers and Geotechnics*, vol. 55, pp. 290–305, 2014.

[30] R. C. Liu, S. Lou, X. J. Li, G. S. Han, and Y. J. Jiang, "Anisotropic surface roughness and shear behaviors of rough-walled plaster joints under constant normal load and constant normal stiffness conditions," *Journal of Rock Mechanics and Geotechnical Engineering*, vol. 12, no. 2, pp. 338–352, 2020.

[31] E. K. Hou, T. Cong, X. S. Xie, and J. B. Wei, "Ground surface fracture development characteristics of shallow double coal seam staggered mining based on particle flow," *Journal of Mining and Strata Control Engineering*, vol. 2, no. 1, pp. 16–24, 2020.

[32] X. R. Liu, Z. Y. Deng, Y. Q. Liu, Y. M. Lu, S. L. Liu, and Y. F. Han, "Macroscopic and microscopic analysis of particle flow in pre-peak cyclic direct shear test of rock joint," *Journal of China Coal Society*, vol. 44, no. 7, pp. 2103–2115, 2019.

[33] X. R. Liu, B. Xu, J. H. Huang et al., "Macro-meso shear mechanical behaviors of coalescent rock joints with different morphologies," *Chinese Journal of Geotechnical Engineering*, vol. 43, no. 3, pp. 406–415, 2021.

[34] Y. F. Ge, H. M. Tang, M. A. M. Ez Eldin, L. Q. Wang, Q. Wu, and C. G. Xiong, "Evolution process of natural rock joint roughness during direct shear tests," *International Journal of Geomechanics*, vol. 17, no. 5, pp. 1–10, 2017.

[35] J. W. Park and J. J. Song, "Numerical method for the determination of contact areas of a rock joint under normal and shear loads," *International Journal of Rock Mechanics and Mining Sciences*, vol. 58, pp. 8–22, 2013.

[36] Y. F. Chen, H. Lin, X. Ding, and S. J. Xie, "Scale effect of shear mechanical properties of non-penetrating horizontal rock-like joints," *Environmental Earth Sciences*, vol. 80, no. 5, pp. 192–202, 2021.

[37] X. Zhang, H. Lin, Y. X. Wang, R. Yong, Y. L. Zhao, and S. du, "Damage evolution characteristics of saw-tooth joint under shear creep condition," *International Journal of Damage Mechanics*, vol. 30, no. 3, pp. 453–480, 2021.

[38] X. Fan, Z. Y. Deng, Z. M. Cui, Z. M. He, and H. Lin, "A new peak shear strength model for soft-hard joint," *Rock and Soil Mechanics*, vol. 42, no. 7, pp. 1–10, 2021.

[39] Y. J. Jiang, Y. Q. Chen, X. Z. Cheng et al., "Experimental study on shear behavior and acoustic emission characteristics of nonpersistent joints," *Geofluids*, vol. 2020, 10 pages, 2020.

[40] Y. J. Jiang, Y. H. Wang, P. Yan, H. Luan, and Y. Q. Chen, "Experimental investigation on the shear properties of heterogeneous discontinuities," *Geotechnical and Geological Engineering*, vol. 37, no. 6, pp. 4959–4968, 2019.

[41] X. Z. Cheng, H. J. Luan, Y. J. Jiang, S. H. Zhang, and C. Y. Jia, "Experimental study on shear behavior and failure mechanism of bolted heterogeneous rock joints under different anchorage conditions," *Geofluids*, vol. 2021, 14 pages, 2021.

[42] J. Yoon, "Application of experimental design and optimization to PFC model calibration in uniaxial compression simulation," *International Journal of Rock Mechanics and Mining Sciences*, vol. 44, no. 6, pp. 871–889, 2007.

[43] X. G. Liu, W. C. Zhu, Q. L. Yu, S. J. Chen, and K. Guan, "Estimating the joint roughness coefficient of rock joints from translational overlapping statistical parameters," *Rock Mechanics and Rock Engineering*, vol. 52, no. 3, pp. 753–769, 2019.

[44] Y. J. Jiang, P. Yan, Y. H. Wang, H. J. Luan, and Y. Q. Chen, "Numerical investigations on shear behavior and failure mechanism of non-persistent jointed rocks," *Geotechnical and Geological Engineering*, vol. 38, no. 2, pp. 1639–1651, 2020.

[45] Itasca Consulting Group Inc (ICG), *PFC2D Version 4.0: Theory and Background*, Itasca Consulting Group Inc, Minneapolis, 2008.